Current Science
CS 5 (3), 2873-2886 (2025)
Received 13 March 2025 | **Revised 17 April** 2025 | **Accepted 12 May**. 2025 | **Online Available 04 June** 2025
https://doi.org/ 10.52845/CS/2025-5-3-62

Current Science

Current Science

OPEN ACCESS **ISSN(O)2795-8639**

Original Article

Experimental Study on the Influence of Displacement Amplitude and Shear Rate on the Shear Characteristics of Pile-Soil Interface

Lei Shen

Department of Highway and Architecture, Shandong Transport Vocational College, Weifang, Shandong 261206, China

***Corresponding Author: Lei Shen**

Abstract:
The mechanism of pile-soil interface interaction is an important research direction in geotechnical engineering. A large-scale, multifunctional soil-structure cyclic shear tester was utilized to systematically investigate the influence of shear rate and cyclic amplitude on the cyclic shear characteristics of the pile-soil interface. The variation laws of interface shear stress, bulk deformation characteristics, equivalent friction angle, and shear stiffness were analyzed. The experimental results indicate that the shape of the hysteresis curve transitions from a 'shuttle shape' to a 'parallelogram' with the displacement amplitude, and the peak shear stress at the interface exhibits a softening phenomenon. As the shear rate increases, the shear softening phenomenon diminishes. With increasing number of cycles, the peak interface shear stress exhibits a logarithmic decay. The primary characteristic of body deformation is shear shrinkage, which correlates positively with the shear displacement amplitude and negatively with the shear rate. The greater the normal stress, the more pronounced the cumulative vertical displacement becomes. The equivalent friction angle exhibits periodic fluctuations during the experimental process, with its amplitude increasing as the shear displacement amplitude increases. The interface friction angle under low normal stress conditions is larger than that under high normal stress conditions. The interface shear stiffness diminishes as the displacement amplitude increases, and the shear stiffness is lower under high normal stress conditions where the normal stress is greater. The amplitude of shear displacement significantly impacts the cyclic shear characteristics of the pile-soil interface, while the influence of the shear rate is relatively small.

Keywords : **Pile; interface; displacement amplitude; shear rate; shear stress; volume change; equivalent friction angle; shear stiffness**

1. Introduction

Pile foundation engineering is commonly employed in extensive engineering projects, including high-rise buildings, bridges, and docks[1-4]. As an important type of foundation, the load-carrying capacity of pile foundations is closely related to the interaction between the pile and the soil. This interaction not only affects the stability of pile foundations [5], but also dictates the deformation behavior and stress pattern of the adjacent soil[6,7]. The operational and seismic performance of pile foundations is directly influenced by the mechanical properties at the pile-soil interface[8,9]. In civil engineering research, enhancing the interfacial shearing resistance of soil-pile systems and refining foundation design methodologies have emerged as prominent investigation directions, driven by progressive insights into soil-structure interaction mechanisms.

Currently, many studies have focused on the shear characteristics of pile-soil interaction under static conditions. Jukun Guo et al. [10,11]investigated how surface roughness impacts the shear behavior at the pile interface, discovering that alterations in the width and angle of the pile structure's surface groove significantly influenced the peak shear stress, friction angle, and cohesion of the interface. Li et al. [12] conducted direct shear

experiments on the sand-concrete interface, observing that an increase in sand particle size resulted in a reduction in the effective contact area between sand and concrete, consequently causing a decrease in shear stress. Xia et al. [13] conducted a study on the shear mechanical properties of the interface layer between soil and underground structures. he results showed that under high stress conditions, there was a "weakening effect" of the interface layer, while under lower stress conditions, it exhibited a "strengthening effect."

However, direct shear tests under static force cannot fully simulate the complex loads on the pile-soil interface in actual engineering, especially the influence of dynamic loads, which limits its application in practical engineering. In practical engineering, the pile-soil interface frequently undergoes dynamic forces, including those from traffic, wind, and earthquakes, which can cause cyclic stresses in the pile-soil interface and affect its mechanical properties [14]. In the recent period, numerous cyclic shear tests have been conducted by scholars both domestically and internationally on the pile-soil interface, revealing the deformation characteristics and strength changes under cyclic loading. For example, Wang et al. [15] employed a large-scale dynamic direct shear apparatus to assess the dynamic shear response at the red clay-concrete interface, observing softening characteristics and anisotropy at various normal stress intensities. In a separate study, Wang et al. [16] investigated the cyclic shear properties of the pile-soil interface under constant stiffness conditions, revealing notable weakening in both interface shear stress and shear stiffness throughout the experimental procedure. Liu et al. [17] conducted shear tests utilizing sand with diverse particle morphologies and geogrids, revealing a profound connection between interface shear strength, soil deformation, and the uniformity of particle shapes.

Research has shown that mechanical behaviors such as interface friction characteristics, shear strength, and hysteresis effects are significantly affected by the shear rate. Experimental investigations of sand-geogrid interfacial behavior have demonstrated rate-dependent frictional characteristics, where shear velocity variations significantly modulate interfacial resistance magnitudes during direct shear testing [18,19]. Wang et al. [20] performed shear tests on concrete, sand, and cohesive soil, observing that with the rise of shear rate, soil shear dilation and strength declined. Evidently, in-depth research on the shear rate's impact on the pile-soil interface mechanics is crucial for pile foundation design and construction.

In summary, current geotechnical literature reveals significant gaps in understanding strain rate dependencies of soil-pile interfacial mechanics, with particularly insufficient characterization of cyclic loading behavior under variable shear rate conditions. Utilizing a large-scale, multifunctional soil-structure cyclic shear testing device, this article conducts a comprehensive investigation into the impacts of shear rate and cyclic amplitude on the cyclic shear behavior of the pile-soil interface, uncovering their effects on shear stress, deformation patterns, friction angle, and shear stiffness. The research findings provide data support for understanding the mechanism of pile-soil interface under dynamic loading, and offer references for the design and construction of pile foundations.

1 Experimental

1.1 Experimental Equipment

As shown in Figure 1, the equipment utilized in this experiment is a large-scale, multifunctional soil-structure cyclic shear tester developed independently. The device incorporates a shear box dimensioned at 160 mm (L) x 160 mm (W) x 85 mm (D), complemented by a lower variant with dimensions of 200 mm (L), 160 mm (W), and 85 mm (D). The increased length of the lower shear box in the shear plane, relative to its upper counterpart, facilitates uniformity in the shear area during testing, thereby mitigating potential discrepancies in test outcomes. In the experiment, the upper shear box remains fixed in position, whereas the lower shear box undergoes horizontal displacement under the force exerted by the servo motor. To reduce friction in the experiment, a sliding track and pulley system are incorporated at the base of the lower shear box. This setup facilitates smooth horizontal movement. Additionally, vertical pressure is exerted on the soil contained within the upper shear box through the use of an air compressor connected to a transmission rod. This method ensures controlled and precise application of load to the soil sample.

Displacement and stress measurements in both the shear and normal directions are captured by corresponding sensors and ultimately recorded through a computer system for collecting data.

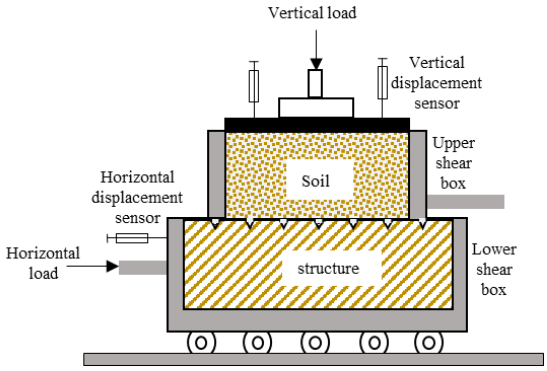

Figure 1 Schematic diagram of cyclic shear

1.2 Experimental Materials

For this experiment, Xiamen standard sand was utilized, as illustrated in Figure 2(a). The particle size distribution, spanning from 0.08 to 2 mm, is depicted in Figure 3. The sand has a uniformity coefficient (Cu) of 2.43 and a curvature coefficient (Cc) of 1.003, and a median particle size d_{50} of 0.96 mm. To simulate the irregularity of the pile surface, a structured surface with engraved grooves was positioned within the lower shear box. Figure 2(b) displays the groove pattern on the surface of the structure.

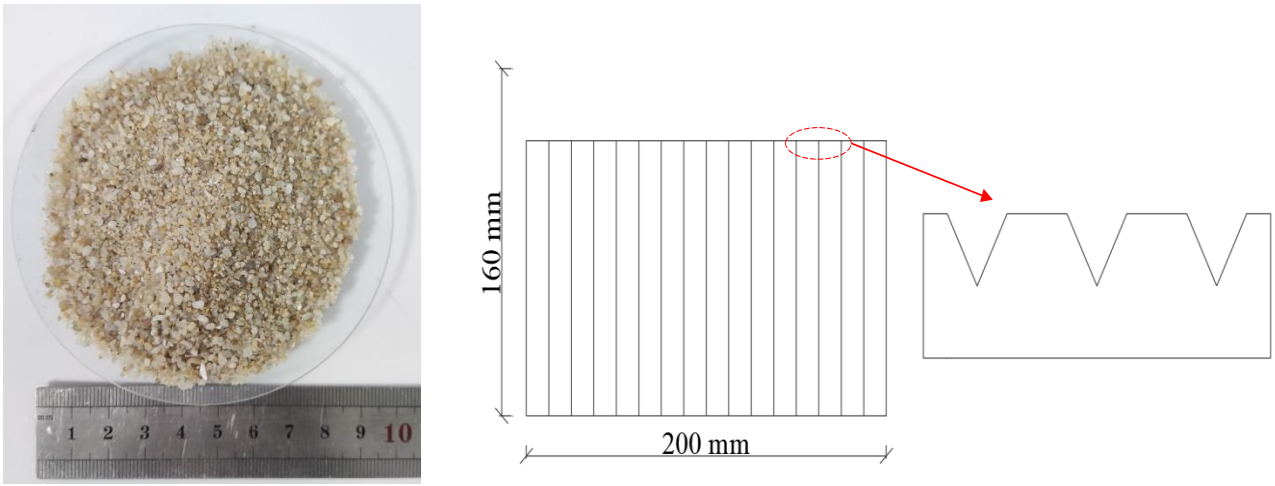

(a) (b)

Figure 2 Experimental Materials (a) Experimental sand; (b) Groove design of structure

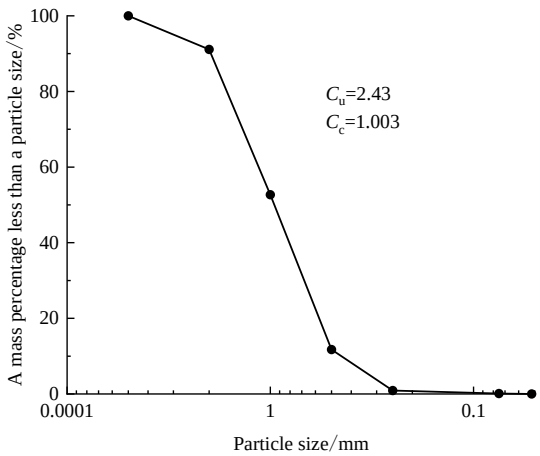

Figure 3 Graph representing the cumulative distribution of particle sizes

1.3 Experimental Plan

To systematically investigate the macroscopic mechanics and volumetric response of cyclic shear at the pile-soil interface, reference was made to relevant literature [18,21,22]. Cyclic shear tests were conducted under varying shear rates (0.5, 1, 2 mm/min) and shear displacement amplitudes (1, 3, 5 mm). The experiment involved 10 cyclic shear cycles, with normal stress levels set at 50 kPa (representing a low stress level) and 200 kPa (representing a high stress level). The shear loading path is illustrated in Figure 4, where ①→②→③→④ signifies a full loading cycle, with the positive direction of τ_x denoting the initial displacement direction of the shear box. A total of 18 experimental groups were conducted, with the specific experimental plan detailed in Table 1.

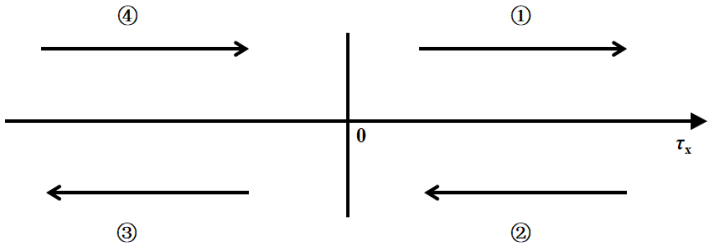

Figure 4 Loop loading path

Table 1 Experimental Plan

Shear displacement amplitude Δu/mm	Shear rate v/mm·min^{-1}	*Normal stress* σ_n/kPa	*Number of cycles N*
1	0.5	50、200	10
3	1		
5	2		

2 Results and Discussion

2.1 Interface Shear Stress

Figures 5-7 show the relationship between interface shear stress and shear displacement at varying shear rates and amplitudes. Figures 5(a)-7(a) are for a low normal stress of 50 kPa, Figures 5(b)-7(b) are for a high normal stress of 200 kPa, and Figures 5(c)-7(c) present the main curve linking maximum shear stress and displacement amplitude [23]. The relationship between cyclic shear stress and shear displacement at the pile-soil interface shows nonlinear features, creating sealed hysteresis loops with each cycle. Moreover, the peak shear stress under forward loading and the peak shear stress under reverse loading are not symmetrically equal within the same cycle. This phenomenon, termed shear anisotropy, arises due to the anisotropic nature of sand particles during the shearing process. Research on the cyclic shear properties of sand and geogrids by Wang et al. [24] and Liu et al. [18,25] also leads to similar findings.

By analyzing the relationships between shear stress and shear displacement across various shear displacement amplitudes, it is found that at small amplitudes (Δu = 1 mm), the hysteresis loop is shuttle-shaped. As the amplitude of displacement grows larger, the shape of the hysteresis loop transforms into a flatter parallelogram, with greater displacement amplitudes leading to flatter hysteresis curves. This suggests that the shear displacement at the pile-soil interface has not yet reached peak strength in the direct shear test at 1 mm. With increasing shear displacement, the interface shear stress continues to increase, reaching peak shear stress at the interface. The main curves in Figures 5(c)-7(c) show little difference in shear stress between cases where the amplitude of shear displacement Δu is 3 mm and 5 mm, which corroborates the experimental findings.

Comparing the shear stress-shear displacement relationships across various shear velocities reveals no significant differences in hysteresis curve shapes across various shear displacement amplitudes. This indicates that the effect of the shear velocity on the hysteresis curve is

comparatively insignificant, with its extent primarily depending on the displacement amplitude and stress level. At low shear rates (v = 0.5 mm/min), the interface shear stress initially increases and then decreases with the rise in displacement amplitude, exhibiting a pronounced shear softening phenomenon. As the shear velocity increases, this phenomenon becomes less significant, with the shear weakening effect being more evident at 200 kPa compared to 50 kPa, particularly in the reverse shear direction.

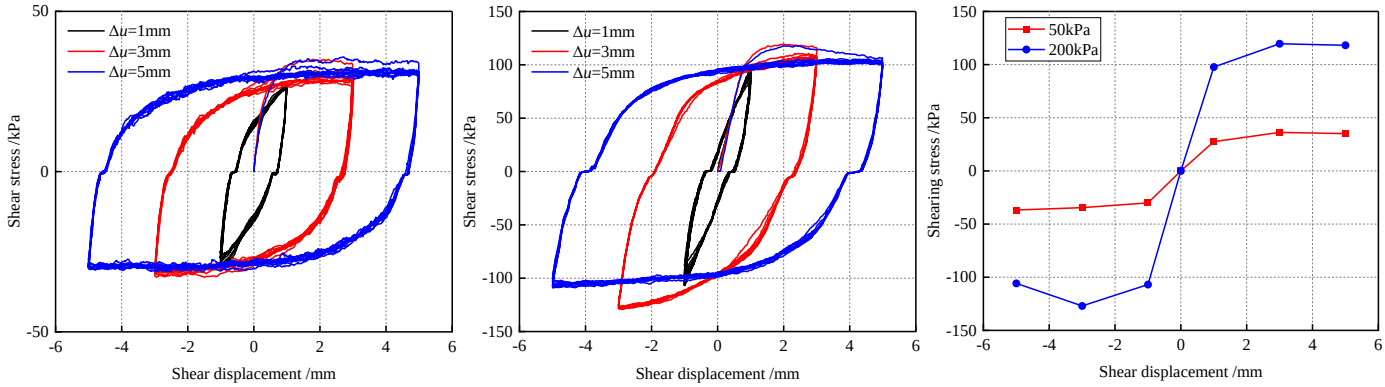

(a) (b) (c)

Figure 5 Correlation between shear stress and shear displacement at a shear velocity of 0.5 mm/min (a) 50 kPa (b) 200 kPa (c) main curve

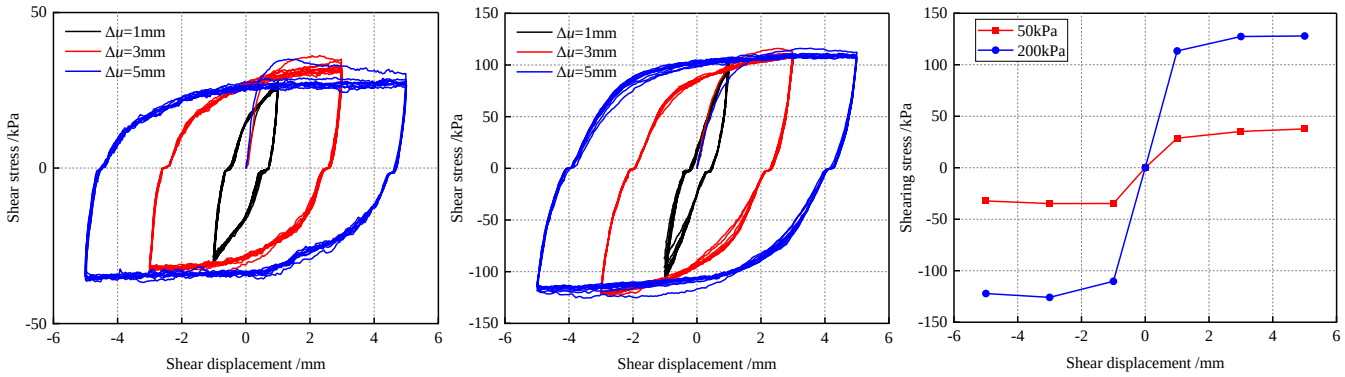

(a) (b) (c)

Figure 6 Correlation between shear stress and shear displacement at a shear velocity of 1 mm/min (a) 50 kPa (b) 200 kPa (c) main curve

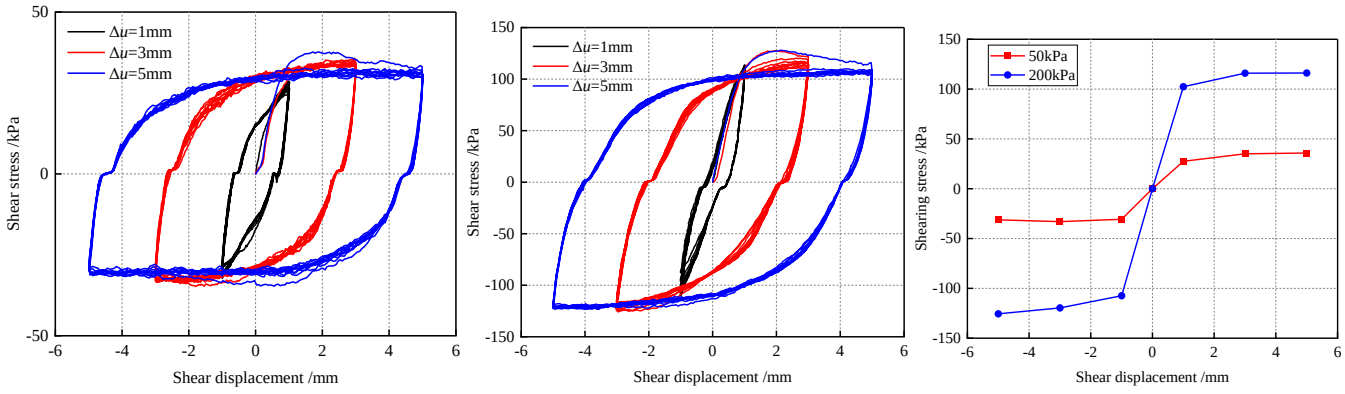

(a) (b) (c)

Figure 7 Correlation between shear stress and shear displacement at a shear velocity of 2 mm/min (a) 50 kPa (b) 200 kPa (c) main curve

To clearly analyze the relationship between shear stress and cycle number under various working conditions, the maximum shear stress observed in both the forward and reverse shear directions of

each cycle is summed and averaged to determine the peak shear stress τ_{mi} at the interface. The calculation formula is:

$$\tau_{mi} = \frac{\tau_{ai} + \tau_{bi}}{2} \quad (1)$$

In the formula, τ_{ai} and τ_{bi} represent the maximum shear stresses in both the positive and negative directions of shear during the *i*-th cycle, respectively; τ_{mi} is the peak shear stress in the i-th cycle.

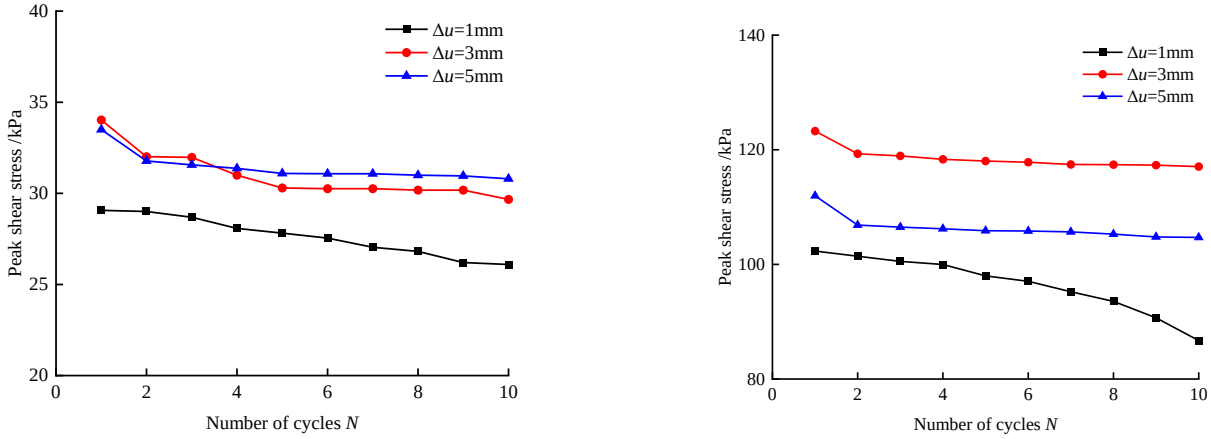

Figure 8 Correlation between shear stress and the quantity of cycles at a shear velocity of 0.5 mm/min (a) 50kPa (b) 200kPa

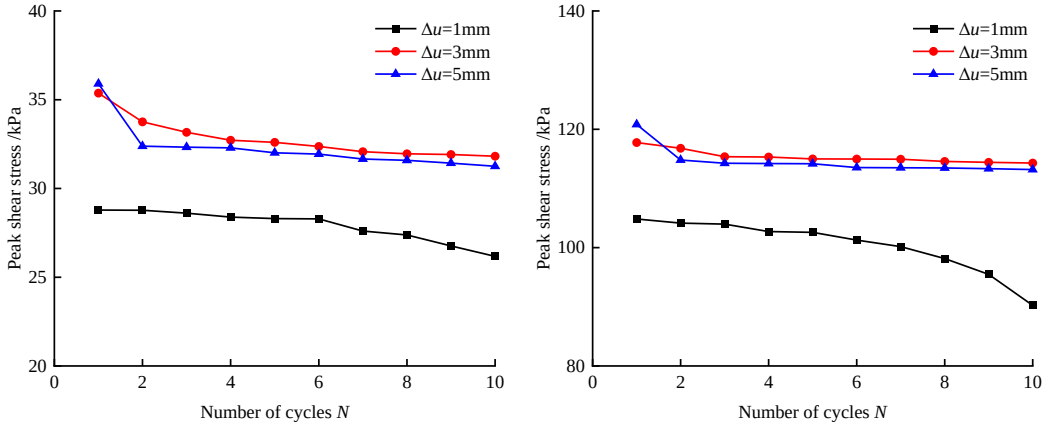

Figure 9 Correlation between shear stress and the quantity of cycles at a shear velocity of 1 mm/min (a) 50kPa (b) 200kPa

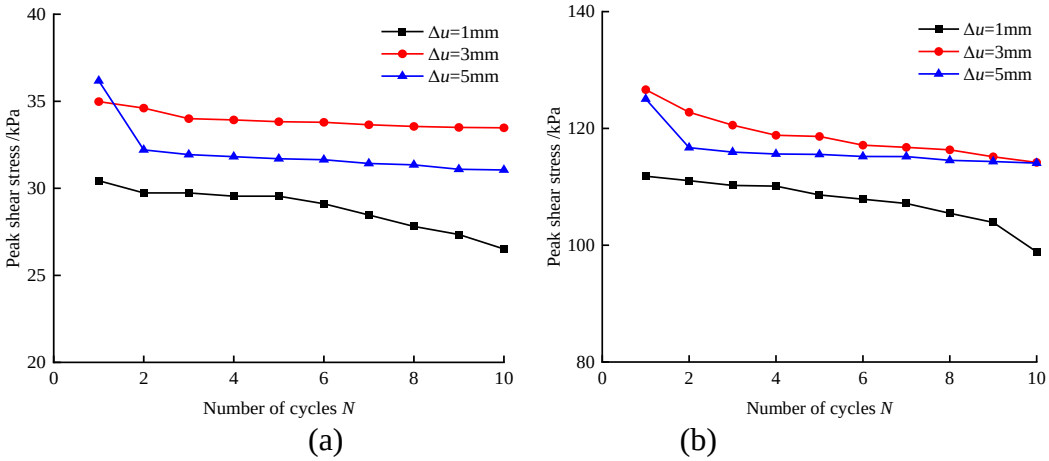

Figure 10 Correlation between shear stress and the quantity of cycles at a shear velocity of 2 mm/min (a) 50kPa (b) 200kPa

Figures 8 to 10 depict the correlation between the maximum shear stress at the interface and the quantity of cycles across diverse operational scenarios. It is noted that with an increase in the quantity of cycles, the maximum shear stress at the interface undergoes varying levels of reduction, showcasing a cyclic weakening effect. The maximum shear stress at the interface reaches its lowest point when the displacement amplitude is 1 mm and peaks when the displacement amplitude is 5 mm. Interestingly, the peak shear stress at a displacement amplitude of 5 mm is slightly lower than that at 3 mm, which strongly indicates that the pile-soil interface has reached its ultimate bearing state near 3 mm. As the shear displacement amplitude rises, shear softening emerges at the interface. The degree of peak shear stress attenuation is greater under the condition of a 1 mm displacement amplitude, while the attenuation degree is smaller for larger displacement amplitudes.

Upon comparing the impact of varying shear rates on the maximum shear stress at the interface, it is observed that, under a shear velocity of 0.5 mm/min, the maximum shear stress at the interface undergoes substantial decay as the number of cycles increases. Increasing the shear rate reduces the degree of attenuation. This is due to the fact that, at low shear rates, soil particles near the interface have sufficient time to rearrange and move during the experiment, leading to the formation of new structures. Conversely, at high shear rates, the faster movement of the lower shear box results in relatively smaller relative position changes among soil particles.

From the aforementioned analysis, it is evident that the peak interface shear stress exhibits a decaying trend with increasing number of cycles during cyclic shearing. To better analyze the degree of peak shear stress attenuation under various working conditions, an attenuation factor $E\tau$ is defined as the ratio of the peak shear stress at the ith cycle to that at the first cycle. The calculation formula for $E\tau$ is as follows:

$$E_\tau = \tau_{mi} / \tau_{m1} \qquad (2)$$

The relationship between the attenuation factor and the number of cycles is illustrated in Figure 11. As can be observed, the variation of the attenuation factor with increasing cycle count is nonlinear. By fitting the relationship between these two variables, it was found that a logarithmic function is suitable for characterizing the attenuation degree of the peak interface shear stress during cyclic shearing. As shown in Figure 11, the evolution law can be expressed as follows:

$$E_\tau = 1 - k\ln(N) \qquad (3)$$

In the above equation, k represents the fitting coefficient, which is used to characterize the attenuation rate of the peak interface shear stress. It can be observed that the value of E_τ ranges from 0.85 to 1, which clearly indicates that the maximum attenuation of the peak shear stress after varying numbers of cycles does not exceed 15%. Notably, the attenuation factor exhibits significant nonlinear characteristics during the testing process. In the initial stages of the test, E_τ decreases rapidly, but as the test progresses, the attenuation curve gradually flattens, demonstrating a distinct phased attenuation behavior. Figure 11(a) illustrates the influence of displacement amplitude on the attenuation characteristics. When the displacement amplitude is 3 mm, the fitted curve is positioned at the lowest level, with the largest k value of 0.058, indicating a higher degree and rate of peak shear stress attenuation under this condition. In contrast, under a displacement amplitude of 1 mm, the shear strain is relatively small, and the damage to the soil structure is not fully activated. Meanwhile, under a displacement amplitude of 5 mm, the rearrangement of particles tends to stabilize, resulting in a lower attenuation rate. Figure 11(b) shows that the fitting coefficient k is negatively correlated with the shear rate. As the shear rate increases from 0.5 mm/min to 2 mm/min, the value of k decreases from 0.058 to 0.020.

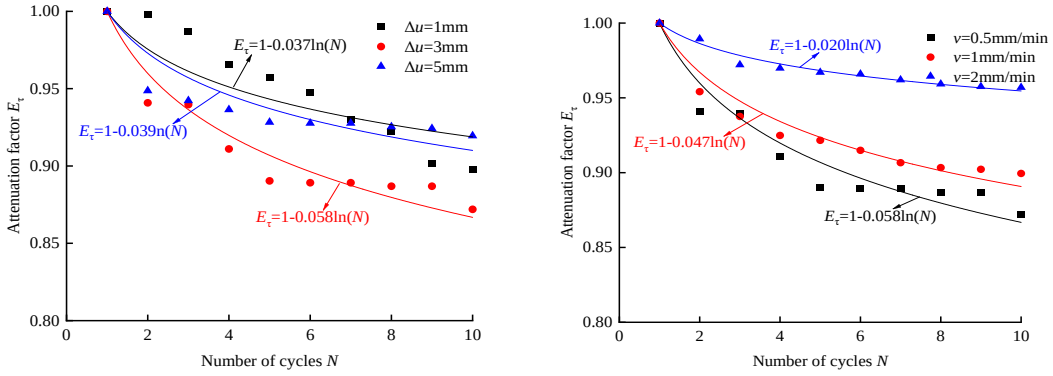

(a) (b)

Figure 11 The relationship between attenuation factor and number of cycles (a) displacement amplitude (b) shear rate

2.2 Volume Change

During the experiment, the extent of soil volume change in proximity to the interface, given the constant shear area, is indicated by the size of the vertical displacement. Negative vertical displacement values indicate volume expansion, while positive values indicate volume compression. To compare different influencing factors horizontally, the control variable method was employed to assess the vertical displacement of the soil during the experimental process. Figure 12 depicts the relationship between vertical displacement and shear displacement for various displacement amplitudes, with a normal stress (σ_n) of 50 kPa. It is observed that as the experiment progresses, the vertical displacement gradually increases, indicating soil volume reduction and increasing soil density. In the first cycle, the test soil exhibited a complete state of shear shrinkage. As the number of cycles increased, there was an alternating phenomenon of shrinkage and expansion, but overall, the soil volume decreased. As the shear displacement amplitude rises, so does the ultimate vertical displacement of the soil. This is because, with a larger shear displacement amplitude, the relative movement between particles during the cyclic shear process intensifies. This relative displacement leads to a gradual rearrangement of the soil's particle structure, especially the loose particles that fill the original pores, leading to a more compact structure and an augmentation in the soil's vertical displacement.

Figure 13 displays the relationship between vertical displacement and shear displacement (σ_n=200 kPa) at different shear rates, indicating that the overall soil volume also exhibits a gradually decreasing trend. At a shear rate of 0.5 mm/min, the vertical displacement measures 1.20 mm, whereas at a shear velocity of 2 mm/min, it diminishes to 0.94 mm. It is noted that as the shear rate increases, the reduction in soil volume diminishes gradually. This is due to the fact that higher shear rates allow less time for soil particles to adjust, which affects the volume change of the soil.

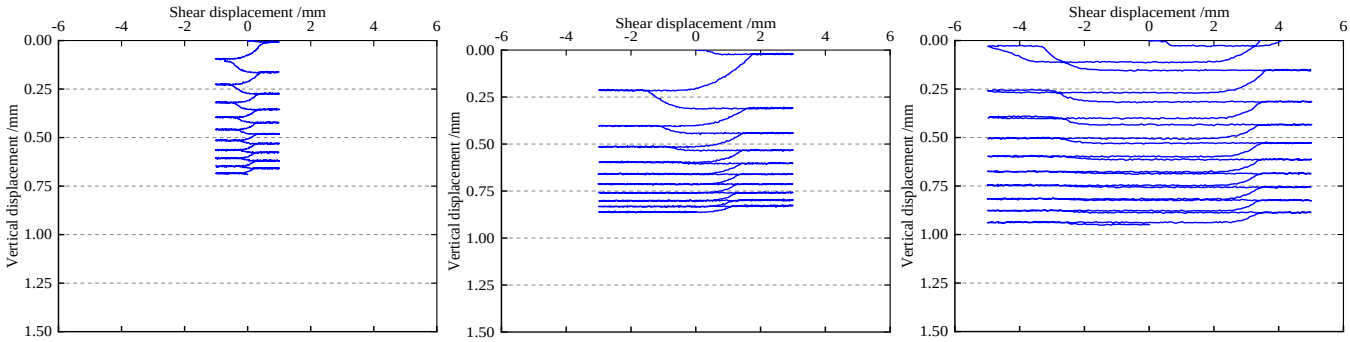

(a) (b) (c)

Figure 12 Vertical displacement-shear displacement relationship under different displacement amplitudes
(a) Δu=1 mm (b) Δu=3 mm (c) Δu=5 mm

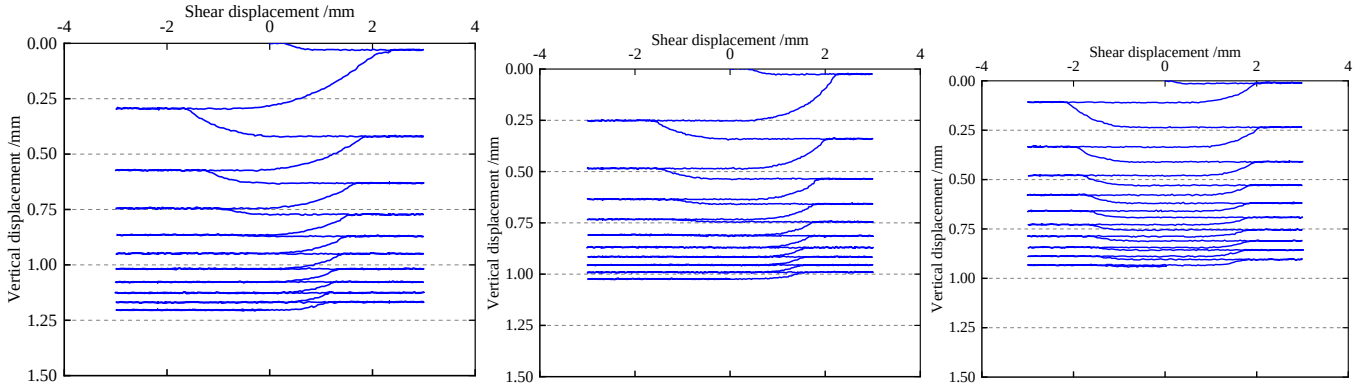

Figure 13 Vertical displacement-shear displacement relationship under different displacement shear rates
(a) *v*=0.5 mm/min (b) *v*=1 mm/min (c) *v*=2 mm/min

Figures 14 and 15 illustrate the relationship curves between cumulative vertical displacement and the number of cycles under 100 kPa and 200 kPa, respectively. Under cyclic shearing, the cumulative vertical displacement of the soil gradually increases, macroscopically manifesting as a progressive reduction in soil volume. During the initial stages of the test, the cumulative vertical displacement increases significantly, but as the number of cycles increases, the change in cumulative vertical displacement gradually stabilizes. Under the same displacement amplitude, the cumulative vertical displacement under a normal stress of 200 kPa is significantly greater than that under 100 kPa. When the normal stress is relatively low, the cumulative vertical displacement exhibits minimal variation with increasing displacement amplitude under cyclic shearing, a phenomenon particularly evident at a shear rate of 2 mm/min. Under the same displacement amplitude, the cumulative vertical displacement of the soil gradually decreases with increasing shear rate, with the shear rate at a displacement amplitude of 1 mm having the most pronounced effect on the cumulative vertical displacement.

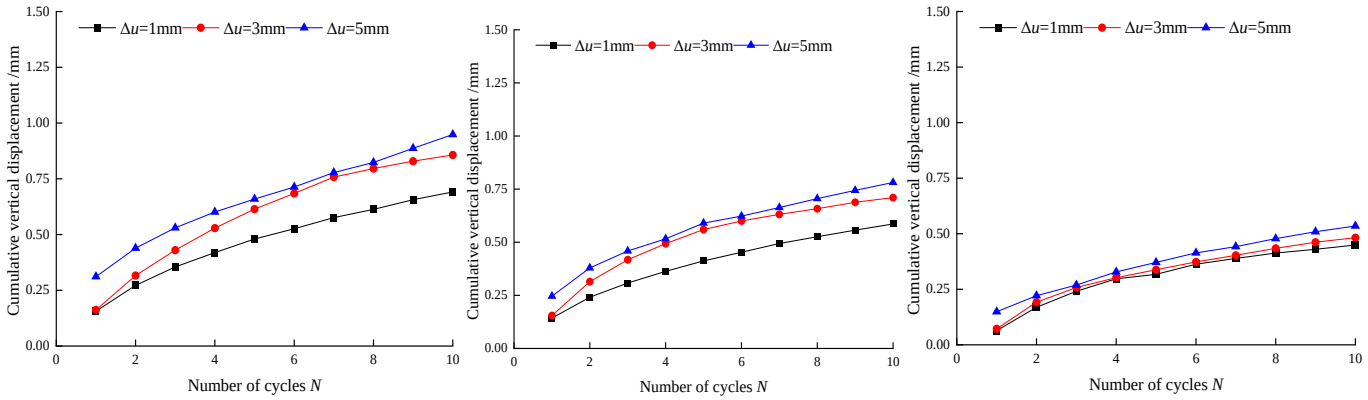

Figure 14 The relationship between cumulative vertical displacement and number of cycles under 100 kPa
(a) v = 0.5 mm/min (b) v = 1 mm/min (c) v = 2 mm/min

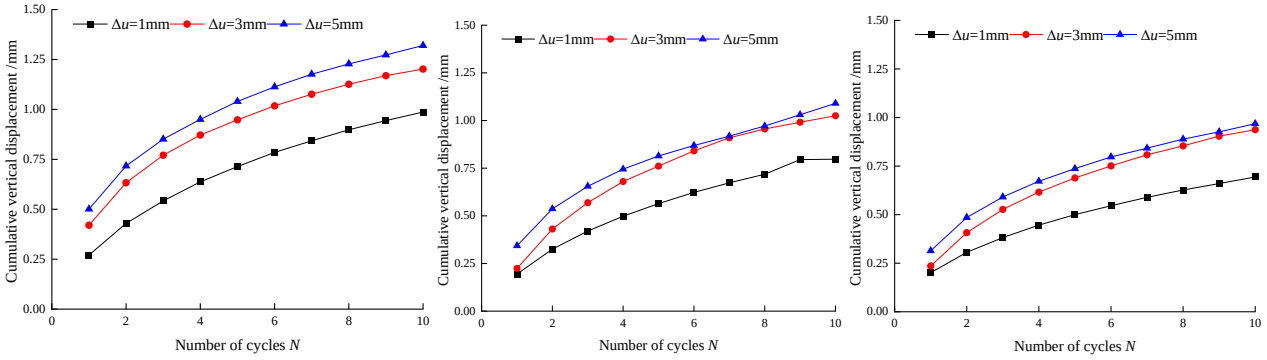

(a) (b) (c)

Figure 15 The relationship between cumulative vertical displacement and number of cycles under 200 kPa
(a) v = 0.5 mm/min (b) v = 1 mm/min (c) v = 2 mm/min

2.3 Interface Equivalent Friction Angle

Utilizing the Mohr-Coulomb shear strength criterion, the notion of an equivalent friction angle is employed to examine the cyclic shear behavior at the pile-soil interface [26-28]. The calculation formula is presented below:

$$\varphi^* = \arctan\left(\frac{\tau}{\sigma_n}\right) \quad (4)$$

Figure 16 demonstrates how the equivalent friction angle at the pile-soil interface varies under different operational conditions. It is noted that the equivalent friction angle undergoes periodic variations within a defined range as the experiment advances. With an increasing number of cycles, there is a minimal shift in the equivalent friction angle. At a shear displacement amplitude of 1 mm, the equivalent friction angle exhibits minor fluctuations, spanning from -31° to 31°, with a peak value of -31.48°. When the shear displacement amplitude reaches 3 mm, the fluctuations in the equivalent friction angle widen, ranging from -36°to 36°. However, when the displacement amplitude is 5 mm, the fluctuation range of the equivalent friction angle is roughly the same or slightly reduced compared to that of 3 mm, which aligns with the variation law of shear stress with displacement amplitude. The impact of altering the shear rate on the equivalent friction angle is minimal, suggesting that the shear rate has a relatively insignificant effect on the equivalent friction angle. This is because the friction angle is an inherent property of the pile-soil interface, primarily related to factors such as soil particle size, particle size distribution, soil compactness, stress history, and interface roughness.

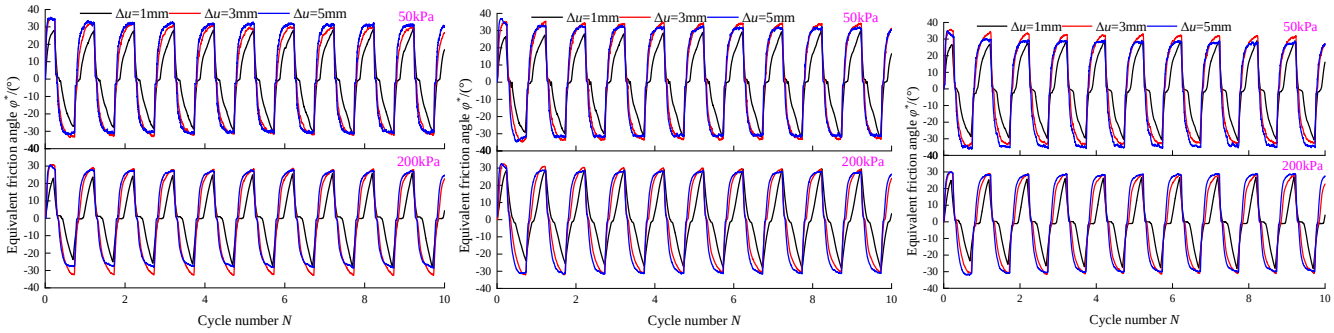

(a) (b) (c)

Figure 16 Variation law of equivalent friction angle
(a) *v*=0.5 mm/min (b) *v*=1 mm/min (c) *v*=2 mm/min

To further investigate, the maximum equivalent friction angles in the forward and reverse shear directions under various operating conditions were summed and averaged to determine the interface friction angle. Figure 17 shows the friction angle at the pile-soil interface under varying test conditions. It is noted that the interface friction angle increases slightly with a

higher shear rate and demonstrates a more noticeable pattern of change with an increased displacement amplitude. At a displacement amplitude of 1 mm, the interface friction angle primarily falls between 27° and 31°. As the displacement amplitude rises, the interface friction angle shifts to a range of 31° to 36°. Furthermore, the increase in displacement amplitude results in a more significant change in the interface friction angle under low normal stress (50 kPa) compared to high normal stress (200 kPa). For instance, taking the shear rate of 1 mm/min as an example, the interface friction angle under 50 kPa increases from 30.0° to 35.8°, while the interface friction angle under 200 kPa only increases from 29.2°to 32.1°.

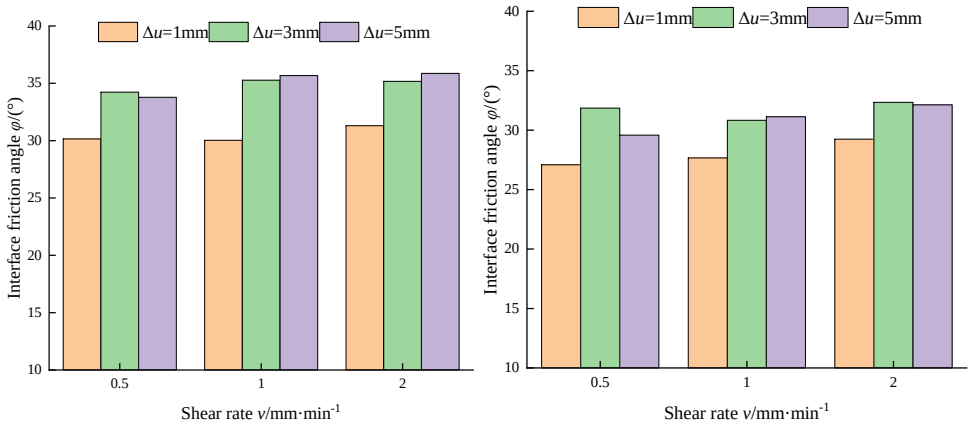

(a) **(b)**

Fig.17 Variation law of interface friction angle
(a) 50 kPa (b) 200 kPa

2.4 Interface Shear Stiffness

Interface shear stiffness is a key parameter that characterizes the dynamic mechanical behavior and response characteristics of soil-structure interfaces, extensively utilized in the study of soil-structure interactions. It reflects the soil's deformation capacity and energy dissipation characteristics under shear action and serves as a fundamental mechanical indicator for evaluating the stability and durability of soil-structure systems [29-31]. Figure 18 presents a classic diagram of the interface shear stiffness calculation, and its calculation formula is:

$$K = \frac{\tau_a + \tau_b}{2\Delta u} \quad (5)$$

In the formula, τ_a and τ_b are the maximum shear stresses corresponding to the amplitude of the shear potential in the positive and negative shear directions, respectively; Δu is the amplitude of shear displacement.

Shown in figure 19 is the connection between interface shear stiffness and cycle count across different operational scenarios. Observations indicate that throughout the experimental process, there was a reduction in interface shear stiffness, though the decrease was slight in magnitude. With all other experimental conditions remaining constant, adjustments to the shear rate resulted in fluctuations in interface shear stiffness around 30 MPa·m^{-1}, suggesting a minimal impact of the shear rate on it. A comparison of shear stiffness under different shear displacement amplitudes revealed that the larger the displacement amplitude, the smaller the interface shear stiffness. Specifically, at a displacement amplitude of 5 mm, the interface shear stiffness reached a minimum of 6.3 MPa·m^{-1}, indicating that under large displacements, more energy is consumed during the interface shear process to overcome particle slip and contact friction, resulting in lower shear stiffness. The shear stiffness under high normal stress (200kPa) was significantly greater than that under low normal stress. This is because under high normal stress, particles undergo a certain degree of fragmentation and rearrangement, altering the mechanical properties of the interface. Although particle fragmentation may weaken the shear resistance to some extent, it can also manifest as an overall increase in interface stiffness due to the embedding effect of particles and the improvement of interface density.

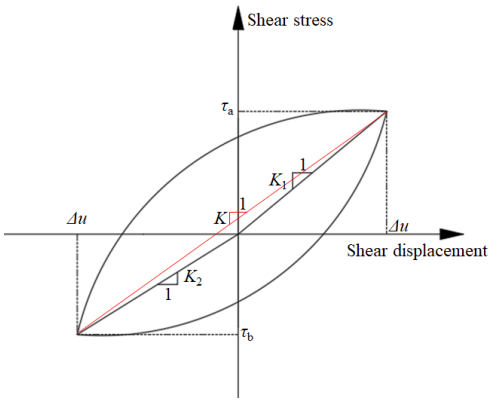

Figure 18 Schematic diagram of shear stiffness calculation for hysteresis curve

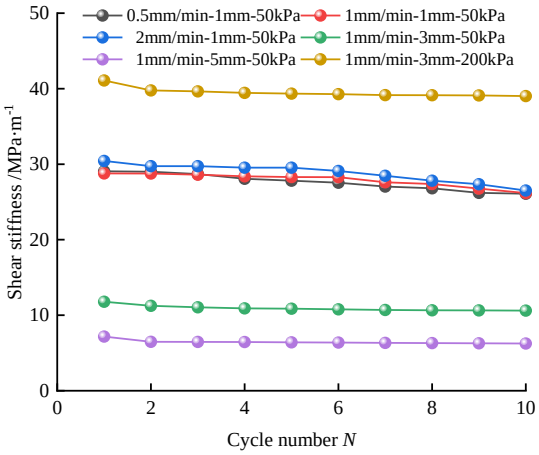

Figure 19 The connection between interface shear stiffness and the quantity of cycles

2.5 Discussion

This article examines the mechanical behavior of the pile-soil interface at shear rates of 0.5, 1, and 2 mm/min. The study reveals that the impact of these shear rates on the pile-soil interface is restricted and can be considered negligible. Xu et al. [32] argue that shear rates not exceeding 7 mm/min have an insignificant effect on the direct shear testing of the reinforced soil interface. It's important to note that the shear properties of the interface at extremely low (<0.5 mm/min) or high (>2 mm/min) shear rates remain inadequately studied, preventing definitive conclusions. Therefore, additional study is needed to explore how shear rate impacts the mechanical behavior of the pile-soil interface, improving our knowledge of the mechanical interactions between piles and soil. Furthermore, the magnitude of shear displacement significantly affects the cyclic shear characteristics of the pile-soil interface. The shape of the hysteresis loop in the shear stress-shear displacement relationship varies with changes in displacement amplitude, and both soil deformation and interface shear stiffness are influenced to different extents by variations in displacement amplitude.

3 Conclusions

This study investigated the shear characteristics and mechanical behavior of the pile-soil interface through cyclic shear tests conducted under varying displacement amplitudes and shear rates. The principal findings are as follows :

(1) As the amplitude of shear displacement increases, the shape of the hysteresis curve transitions from a 'shuttle-shaped' to a 'parallelogram', with a corresponding increase in shear stress. At low shear rates, interface shear stress exhibits a softening behavior, which is more pronounced at high stress levels. As shear rate rises, the shear softening ebb. The peak interface shear stress shows logarithmic decay as cycles increase, with maximum attenuation at 3 mm displacement amplitude. Moreover, higher shear rates slow the attenuation of peak interface shear stress.

(2) Under varying experimental conditions, the soil adjacent to the interface undergoes shear-

induced compaction. The degree of this compaction intensifies with an increase in shear displacement amplitude but diminishes with an increase in shear rate. The cumulative vertical displacement becomes more pronounced under higher normal stress conditions.

(3) The equivalent friction angle exhibits a rhythmic pattern of variation throughout the experimental process, with the magnitude of this variation augmenting as the shear displacement amplitude grows. The interface friction angle shows significant variation with increasing displacement amplitude, being higher under low normal stress than high normal stress. In contrast, shear rate has a relatively minor effect on the interface friction angle.

(4) As the cycle count accumulates, the interface shear stiffness undergoes a slight decrement. Larger shear displacement amplitudes are associated with lower interface shear stiffness. Under conditions of high normal stress and low shear displacement amplitudes, the interface shear stiffness is relatively higher.

Conflict of Interest statement

The authors declare no conflict of interest.

Funding statement

No external funding received.

References

1. Hou X, Chen J, Liu Y, Rui P, Zhao J, Zhang S, et al. Field observation of the thermal disturbance and freezeback processes of cast-in-place pile foundations in warm permafrost regions. Research in Cold and Arid Regions. 2023;15(1):18-26.
2. Zhang CC, Feng ZJ, Zhang C, Wang FC, Wang XQ. Study on the seismic responses and differences between rock-socketed single pile and pile group foundations under different scour depths. Soil Dyn Earthq Eng. 2024;187:14. http://dx.doi.org/10.1016/j.soildyn.2024.108971
3. Gao X, Liu HL, Li LP, Fan HY, Li SG, Wang SC. Analysis of tunnel collapse mechanism due to dislocation and fracture of the surrounding rock block, and a method to predict the collapse height. Physics of Fluids. 2024;36(11). http://dx.doi.org/10.1063/5.0242607
4. Wang JT, Gao X, Liu HL, Dai L, Li X, Ren ZT, et al. Characteristic analysis of tunnel collapse arch in weak rock mass. Physics of Fluids. 2024;36(9). http://dx.doi.org/10.1063/5.0226218
5. Basha A, Elmorsy S, Mansour W, Ramadan B. Effect of the pile cap length and the soil relative density on the pile cap - pile - dense soil interaction: Experimental investigation. Case Stud Constr Mater. 2024;20:14. http://dx.doi.org/10.1016/j.cscm.2024.e03169
6. Cui CY, Meng K, Xu CS, Wang BL, Xin Y. Vertical vibration of a floating pile considering the incomplete bonding effect of the pile-soil interface. Comput Geotech. 2022;150:10. http://dx.doi.org/10.1016/j.compgeo.2022.104894
7. Varghese R, Boominathan A, Banerjee S. Stiffness and load sharing characteristics of piled raft foundations subjected to dynamic loads. Soil Dyn Earthq Eng. 2020;133:15. http://dx.doi.org/10.1016/j.soildyn.2020.106117
8. Hui X, Yinsheng ZOU, Shouping S. On the Dynamic Interaction Designing of Pile-supported Structures under Seismic Load. Journal of Hunan University Natural Sciences. 2007;34(11):1-5.
9. Shi XH, Lai JX, Ma C, He SY, Li BL, Liu T, et al. Soil disturbance effects of pile-reinforced metro foundation subjected by tunnelling beneath: field investigation and model tests. Structures. 2024;69:13. http://dx.doi.org/10.1016/j.istruc.2024.107280
10. Guo JK, Wang XW, Lei SY, Wang R, Kou HL, Wei DK. Effects of Groove Feature on Shear Behavior of Steel-Sand Interface. Adv Civ Eng. 2020;2020:15. http://dx.doi.org/10.1155/2020/9593187
11. Guo J, Lei S, Wang R, Kou H, Rong W. Study on Interface Shear Mechanism between Structures and Standard Sand. Chinese Journal of Underground Space and Engineering. 2020;16(3):722-33.
12. Li T, Chen X, Chen W, Yuan X. Experimental study on interface frictional property between sand and concrete pipe jacking. Bulletin of Geological Science and Technology. 2021;40(6):178-84.
13. Xia H, Zhou G, Du Z. Experimental study of the soil-underground structure interfacial layer effect. Journal of China University of Mining & Technology. 2011;40(6):846-51.
14. Zeng WX, Ying MJ, Liu FY. Investigation on the cyclic shear response of stereoscopic geogrid-reinforced coarse-grained soil interface. Transp Geotech. 2023;38:12. http://dx.doi.org/10.

1016/j.trgeo.2022.100905
15. Wang X, Cheng H, Yan P, Zhang JS, Ding Y. The influence of roughness on cyclic and post-cyclic shear behavior of red clay-concrete interface subjected to up to 1000 cycles. Construction and Building Materials. 2021;273. http://dx.doi.org/10.1016/j.conbuildmat.2020.121718
16. Wang R, Guo JK, Lei SY, Wang XW, Rong WT, Yu ZH. A study on the cyclic shear and particle breakage characteristics of the interface between steel and calcareous sand. Marine Georesources & Geotechnology. 2023;41(12):1426-39. http://dx.doi.org/10.1080/1064119x.2022.2146024
17. Liu FY, Ying MJ, Yuan GH, Wang J, Gao ZY, Ni JF. Particle shape effects on the cyclic shear behaviour of the soil-geogrid interface. Geotext Geomembr. 2021;49(4):991-1003. http://dx.doi.org/10.1016/j.geotexmem.2021.01.008
18. Liu F, Wang P, Wang J, Cai Y. Cyclic and post-cyclic shear behavior of sand-geogrid interface under different shear rates. Chinese Journal of Rock Mechanics and Engineering. 2016;35(2):387-95.
19. Sweta K, Hussaini SKK. Effect of shearing rate on the behavior of geogrid-reinforced railroad ballast under direct shear conditions. Geotext Geomembr. 2018;46(3):251-6. http://dx.doi.org/10.1016/j.geotexmem.2017.12.001
20. Wang Y, Zhang M, Bai X, Liu J. Experimental research on effect of shear rate on shear strength of clayey soil-concrete interface. Journal of Civil and Environmental Engineering. 2019;41(1):48-54.
21. Feng SJ, Shi JL, Shen Y, Chen HX, Chang JY. Dynamic shear behavior of GMB/CCL interface under cyclic loading. Geotext Geomembr. 2021;49(3):657-68. http://dx.doi.org/10.1016/j.geotexmem.2020.12.002
22. Ying MJ, Liu FY, Wang J, Wang CL, Li MF. Coupling effects of particle shape and cyclic shear history on shear properties of coarse-grained soil-geogrid interface. Transp Geotech. 2021;27:13. http://dx.doi.org/10.1016/j.trgeo.2020.100504
23. Chang JY, Feng SJ. Dynamic shear behaviors of textured geomembrane/nonwoven geotextile interface under cyclic loading. Geotext Geomembr. 2021;49(2):388-98. http://dx.doi.org/10.1016/j.geotexmem.2020.10.010
24. Wang J, Liu FY, Wang P, Cai YQ. Particle size effects on coarse soil-geogrid interface response in cyclic and post-cyclic direct shear tests. Geotext Geomembr. 2016;44(6):854-61. http://dx.doi.org/10.1016/j.geotexmem.2016.06.011
25. Liu F, Zheng Q, Wang J, Ying M. Effects of particle shape on shear behaviors of interface between coarse-grained soil and geogrid. Journal of Civil and Environmental Engineering. 2021;43(6):48-56.
26. Jiang YJ, Zhao Y. Experimental investigation of dry granular flow impact via both normal and tangential force measurements. Geotech Lett. 2015;5(1):33-8. http://dx.doi.org/10.1680/geolett.15.00003
27. Jiang H. Expressing strength criterion in principal stress plane base on equivalent Mohr-Coulomb friction angle. Journal of Central South University of Science and Technology. 2012;43(8):3216-21.
28. Jiang H, Wang XW. A new method to calculate the equivalent Mohr-Coulomb friction angle for cohesive and frictional materials. Int J Numer Anal Methods Geomech. 2011;35(5):630-8. http://dx.doi.org/10.1002/nag.922
29. Li S, Tong Y, Liu F, Chen S. Seismic Response of Reinforced Soil Slope Considering Interface Stiffness Softening under Different Water Content. Journal of Disaster Prevention and Mitigation Engineering. 2023;43(4):862.
30. Wang L, Liu S, Zhao Z, Shen C, Lu Y. Experimental study on dynamic behaviour for soilbag interface using cyclic direct shearing test. Rock and Soil Mechanics. 2021;42(6):1625-34.
31. Fox PJ, Sura JM, Nye CJ. Dynamic Shear Strength of a Needle-Punched GCL for Monotonic Loading. J Geotech Geoenviron Eng. 2015;141(7):10. http://dx.doi.org/10.1061/(asce)gt.1943-5606.0001304
32. Xu C, Meng F. Effects of shear rate and material properties on shear strength of geosynthetic-soil interface. Rock and Soil Mechanics. 2010;31(10):3101-6